Article

Polymer Particles with Various Shapes and Morphologies Produced in Continuous Microfluidic Reactors

Zhihong Nie, Shengqing Xu, Minseok Seo, Patrick C. Lewis, and Eugenia Kumacheva

J. Am. Chem. Soc., **2005**, 127 (22), 8058-8063• DOI: 10.1021/ja042494w • Publication Date (Web): 11 May 2005

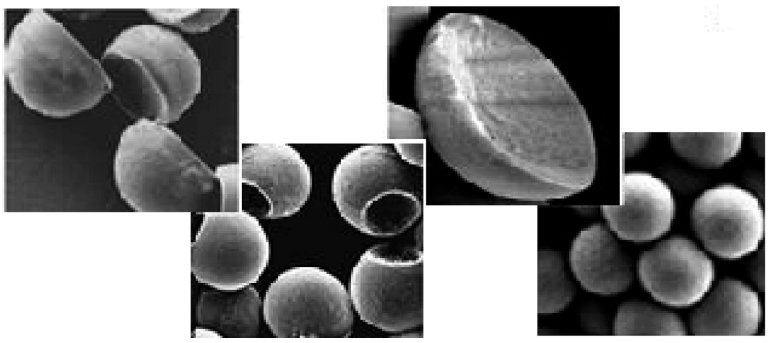

J|A|C|S
ARTICLES
Published on Web 05/11/2005

Polymer Particles with Various Shapes and Morphologies Produced in Continuous Microfluidic Reactors

Zhihong Nie, Shengqing Xu, Minseok Seo, Patrick C. Lewis, and Eugenia Kumacheva*

Contribution from the Department of Chemistry, University of Toronto, 80 Saint George Street, Toronto, Ontario, M5S 3H6 Canada

Received December 14, 2004; Revised Manuscript Received April 7, 2005; E-mail: ekumache@chem.utoronto.ca

Abstract: We report a novel approach to continuous and scalable production of core−shell droplets and polymer capsules in microfluidic devices. The described method is also useful in the synthesis of polymer particles with nonspherical shapes. We used capillary instability-driven break-up of a liquid jet formed by two immiscible fluids. Precise control of emulsification of each liquid allowed for the production of highly monodisperse core−shell droplets with a predetermined diameter of cores and thickness of shells. We also achieved control over the number of cores per droplet and the location of cores in the droplet. We carried out fast throughput photopolymerization of the monomeric shells and obtained polymer particles with various shapes and morphologies, including spheres, truncated spheres and, hemispheres, and single and multicore capsules.

Introduction

We developed a novel single-step approach to continuous microfluidics-based synthesis of highly monodispersed spherical polymer capsules with controlled number of liquid droplets per particle. The described strategy can also be used for the generation of particles with nonspherical shapes such as truncated spheres and hemispheres. We employed laminar flow of three immiscible liquids in a planar microfluidic flow-focusing device[1] to obtain a coaxial jet of silicon oil and monomer in the continuous aqueous phase. Controlled break-up of the coaxial liquid thread led to the production of highly monodipserse droplets with various morphologies. The resultant droplets were continuously photopolymerized in the microfluidic reactor to generate spherical polymer capsules or particles with different shapes.

Polymer particles frequently have applications largely governed by their shapes and morphologies. Microbeads with nonspherical shapes undergo field-induced orientation and assemble in topologically complex lattices.[2−4] Particles with core−shell or multilayer structures are used in coating technologies, optical data storage, security data encryption, and as spherical dielectric resonators.[5−7] Particles with liquid cores (polymer capsules) have applications in the encapsulation of drugs, cells, pesticides, perfumes, liquid inks, paints, and toners.[8−10]

Polymer core−shell microparticles and microcapsules are generally obtained by interfacial polymerization reactions,[10−12] controlled phase separation,[13] layer-by-layer (LBL) deposition of polyelectrolyte multilayers,[8,14] coacervation,[15] and Shirasu porous glass (SPG) monomer emulsification accompanied by batch or continuous polymerization.[12,16] Most of these methods are either expensive or time-consuming,[14,16] or they produce particles with insufficient control over their size distribution and morphology.[11−15] In addition, lack of control over the thickness of capsular walls[8,14,15] and exposure of the contents of cores to the reactants used in the encapsulation process may limit the applications of such particles.[8−14]

(1) Anna, S. L.; Bontoux, N.; Stone, H. A. *Appl. Phys. Lett.* **2003**, *82*, 364−366.
(2) Alargova, R. G.; Bhatt, K. H.; Paunov, V. N.; Velev, O. D. *Adv. Mater.* **2004**, *16*, 1653−1657.
(3) Lu, Y.; Yin, Y.; Xia, Y. *Adv. Mater.* **2001**, *13*, 415−420.
(4) (a) Breen T. L.; Tien J.; Oliver S. R. J.; Hadzic T.; Whitesides G. M. *Science* **1999**, *284*, 948−951. (b) Bowden, N.; Choi, I. S.; Grzybowski, B. A.; Whitesides, G. M. *J. Am. Chem. Soc.* **1999**, *121*, 5373−5391.
(5) (a) Soucek, M. D.; Teng, G. H.; Wu, S. B. *J. Coat. Technol.* **2001**, *73*, 117−125. (b) Stubbs, J. M.; Sundberg, D. C. *J. Coat. Technol.* **2003**, *75*, 59−67.
(6) Alteheld, A.; Gourevich, I.; Field, L. M.; Paquet, C.; Kumacheva, E. *Macromolecules* **2005**, *38*, 3301−3306.
(7) (a) Siwick, B.; Kalinina, O.; Kumacheva, E.; Miller, D. R. J. *J. Appl. Phys.* **2001**, *90*, 5328−5334. (b) Pham, H.; Gourevich, I.; Oh, J. K.; Jonkman, J. E. N.; Kumacheva, E. *Adv. Mater.* **2004**, *16*, 516−520.
(8) Peyratout, C. S.; Dähne, L. *Angew. Chem., Int. Ed.* **2004**, *43*, 3762−3783.
(9) (a) Orive, G.; Hernandez, R. M.; Gascon, A. R.; Calafiore, R.; Chang, T. M. S.; De Vos, P.; Hortelano, G.; Hunkeler, D.; Lacik, I.; Shapiro, A. M. J.; Pedraz, J. L. *Nat. Med.* **2003**, *9*, 104−107. (b) Dusseault, J.; Leblond, F. A.; Robitaille, R.; Jourdan, G.; Tessier, J.; Menard, M.; Henley, N.; Halle, J. P. *Biomaterials* **2005**, *26*, 1515−1522.
(10) Benita, S. *Microencapsulation: Methods and Industrial Applications*; Marcel Dekker: New York, 1996.
(11) Pham, H. H.; Kumacheva, E. *Macromol. Symp.* **2003**, *192*, 191−205.
(12) Chu, L. Y.; Xie, R.; Zhu, J. H.; Chen, W. M.; Yamaguchi, T.; Nakao, S. *J. Colloid Interface Sci.* **2003**, *265*, 187−196.
(13) (a) Loxley, A.; Vincent, B. *J. Colloid Interface Sci.* **1998**, *208*, 49−62. (b) Shulkin, A.; Stöver, H. D. H. *Macromolecules* **2003**, *36*, 9836−9839. (c) Dowding, P. J.; Atkin, R.; Vincent, B.; Bouillot, P. *Langmuir* **2004**, *20*, 11374−11379.
(14) (a) Shchukin, D. G.; Ustinovich, E. A.; Sukhorukov, G. B.; Mohwald, H.; Sviridov, D. V. *Adv. Mater.* **2005**, *17*, 468−472. (b) Shi, X. Y.; Caruso, F. *Langmuir* **2001**, *17*, 2036−2042. (c) Antipov, A. A.; Sukhorukov, G. B. *Adv. Colloid Interface Sci.* **2004**, *111*, 49−61.
(15) (a) Nakagawa, K.; Iwamoto, S.; Nakajima, M.; Shono, A.; Satoh, K. *J. Colloid Interface Sci.* **2004**, *278*, 198−205. (b) Quek, C. H.; Li, J.; Sun, T.; Ling, M.; Chan, H.; Mao, H. Q.; Gan, L. M.; Leong, K. W.; Yu, H. *Biomaterials* **2004**, *25*, 3531−3540.
(16) (a) Ma, G. H.; Su, Z. G.; Omi, S.; Sundberg, D.; Stubbs, J. *J. Colloid Interface Sci.* **2003**, *266*, 282−294. (b) Liu, R.; Ma, G. H.; Meng, F. T.; Su, Z. G. *J. Controlled Release* **2005**, *103*, 31−43.

10.1021/ja042494w CCC: $30.25

Nonspherical polymer particles have been synthesized by varying the compositions and properties of continuous and dispersed phases and the reaction temperature.[17] Alternatively, geometric confinement, uniaxial stretching of spherical polymer beads,[3,18] liquid dispersion technique,[2] and microfabrication methods[4,19] have been used to obtain polymer microbeads with various nonspherical shapes.

Synthesis in microfluidic reactors provides a powerful strategy for continuous, reproducible, and scalable production of inorganic, organic, and bio-organic products.[20] Recently, several groups reported continuous synthesis of polymer particles (micropheres, ellipsoids, disks, rods, and tubes) in microfluidic laminar flow reactors.[21,22] To the best of our knowledge, to date the preparation of polymer capsules by means of microfluidics is conducted in a noncontinuous two-stage process which included (i) the generation of core−shell droplets and (ii) batch-type hardening of droplet shells by photopolymerization, solvent evaporation, or gelation.[23] The use of batch processes overshadows the advantages of the microfluidics-based synthesis: the possibility of continuous and reproducible production of highly monodispersed particles[24] with no need for protection of droplets against coalescence.

Here we report continuous "on-the fly" synthesis of polymer spherical capsules and particles with nonspherical shapes in a planar microfluidic reactor. The described approach leads to the production of polymer capsules with precise control over the size of liquid cores, the thickness of shells, and the overall size of the particles, along with optional control over the number of core droplets (later in the text referred to as "cores") per capsule.

Results and Discussion

The microfluidic reactor was fabricated in polyurethane (PU) elastomer by using standard soft-lithography which allowed rapid replication of an integrated microchannel prototype.[25] Masters were prepared with features of SU-8 photoresist (MicroChem, U.S.A.) in bas-relief on silicon wafers. Figure 1a shows a schematic of the generation of droplets in a modified microfluidic flow-focusing device (MFFD).[1] Three immiscible liquids A, B, and C were supplied to the MFFD: a 2 wt % aqueous solution of sodium dodecyl sulfate (liquid C) was supplied from two sides of the microfluidic device; the oil and monomer phases (liquids A and B, respectively) were supplied from the central channels. We used two monomers, tripropyleneglycol diacrylate (TPGDA) or ethyleneglycol dimethacrylate (EGDMA), comprising 4 wt % of photoinitiator 1-hydroxycyclohexyl phenyl ketone (HCPK) and a silicon oil (SO) mixed with 0.2−2.0 wt % of surfactant sorbitan monooleate SPAN 80. We found that an increase in concentration of SPAN 80 above 0.2 wt % only slightly affected viscosity of the silicone oil and interfacial tension between the oil and monomer phases (and hence did not lead to a noticeable change in the size of oil droplets). By contrast, the size of core−shell droplets decreased as SDS concentration in the aqueous phase increased from 0.2 to 1.2 wt % (for this concentration range the value of interfacial tension between the aqueous and monomer phases decreased).

When a pressure gradient acting along the long axis of the MFFD forced three liquids into a narrow orifice (Figure 1a), the monomer stream was pulled away from the top and bottom walls of the PU mold due to the higher affinity of the water phase to the PU elastomer and strong contraction of highly accelerating external phase. Thus, the continuous water phase surrounded the monomer−oil thread which adopted a circular cross-section.[26] The coaxial jet extended into the downstream channel and broke up into segments. Under the action of interfacial tension these segments acquired a spherical shape.

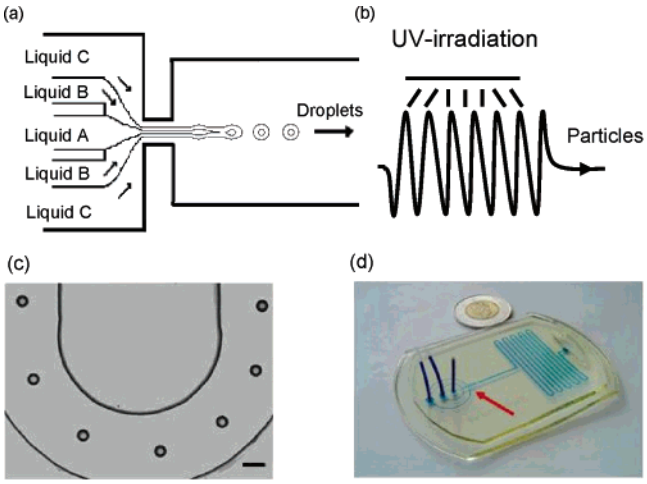

Figure 1. (a) Schematic of production of droplets in MFFD by laminar co-flow of silicone oil (A), monomer (B), and aqueous (C) phases. The orifice had a rectangular shape with width and height of 60 and 200 μm, respectively. (b) Schematic of the wavy channel used for photopolymerization of monomer in core−shell droplets. (c) Optical microscopy image of core−shell droplets flowing in the wavy channel used for in situ monomer photopolymerization. The scale bar is 200 μm. (d) Photograph of a PU microfluidic system. Polyethylene tubing and microchannels are filled with a dye-labeled aqueous solution for increasing contrast of image. Scale bar is 2.5 cm. The arrow is pointing to the orifice.

(17) (a) Skjeltorp, A. T.; Ugelstad, J.; Ellingsen, T. J. *Colloid Interface Sci.* **1986**, *113*, 577−582. (b) Sheu, H. R.; Elaasser, M. S.; Vanderhoff J. W. *J. Polym. Sci., Part A: Polym. Chem.* **1990**, *28*, 653−667. (c) Okubo, M.; Konishi, Y.; Sebki, S.; Minami, H. *Colloid Polym. Sci.* **2002**, *280*, 765−769. (d) Sundberg, D. C.; Casassa, A. P.; Pantazopoulos, J.; Muscato, M. R.; Kronberg, B.; Berg, J. *J. Appl. Polym. Sci.* **1990**, *41*, 1425−1442. (e) Chen, Y. C.; Dimonie, V.; Elaasser, M. S. *Macromolecules* **1991**, *24*, 3779−3787.

(18) (a) Sutera, S. P.; Boylan, C. W. *J. Colloid Interface Sci.* **1980**, *73*, 295−297. (b) Keville, K. M.; Franses, E. I.; Caruthers, J. M. *J. Colloid Interface Sci.* **1991**, *144*, 103−126

(19) Choi, D. G.; Yu, H. K.; Jang, S. G.; Yang, S. M. *J. Am. Chem. Soc.* **2004**, *126*, 7019−7095.

(20) (a) Cheng, J.; Schoffner, M. A.; Mitchelson, K. R.; Kricka, L. J.; Wilding, P. *J. Chromatogr., A* **1996**, *732*, 151−158. (b) Kopp, M. U.; de Mello, A. J.; Manz, A. *Science* **1998**, *280*, 1046−1048. (c) Chan, E. M.; Mathies, R. A.; Alivisatos, A. P. *Nano Lett.* **2003**, *3*, 199−201. (d) Khan, S. A.; Gunther, A.; Schmidt, M. A.; Jensen, K. F. *Langmuir* **2004**, *20*, 8604−8611. (e) Fortt, R.; Wootton, C. R.; de Mello, A. J. *Org. Process Res. Dev.* **2003**, *7*, 762−768. (f) Kobayashi, J.; Mori, Y.; Okamoto, K.; Akiyama, R.; Ueno, M.; Kitamori, T.; Kobayashi, S. *Science* **2004**, *304*, 1305−1308.

(21) Xu, S.; Nie, Z. H.; Seo, M.; Lewis, P.; Kumacheva, E.; Stone, H. A.; Garstecki, P.; Weibel, D. B.; Gitlin, I.; Whitesides, G. M. *Angew. Chem., Int. Ed.* **2005,** *44*, 724−728.

(22) (a) Jeong, W.; Kim, J.; Kim, S.; Lee, S.; Mensing, G.; Beebe. D. J. *Lab Chip* **2004**, *4*, 576−580; (b) Dendukuri, D.; Tsoi, K.; Hatton, T. A.; Doyle, P. S. *Langmuir* **2005**, *21*, 2113−2116.

(23) (a) Loscertales, I. G.; Barrero, A.; Guerrero, I.; Cortijo, R.; Marquez, M.; Ganan-Calvo, A. M. *Science* **2002**, *295*, 1695−1698. (b) Berkland, C.; Pollauf, E.; Pack, D. W.; Kim, K. *J. Controlled Release* **2004**, *96*, 101−111. (c) Kawakatsu, T.; Trägårdh, G.; Trägårdh, C. *Colloids Surf., A* **2001**, *189*, 257−264. (d) Sugiura, S.; Nakajima, M.; Yamamoto, K.; Iwamoto, S.; Oda, T.; Satake, M.; Seki, M. *J. Colloid Interface Sci.* **2004**, *270*, 221−228. (e) Okushima, S.; Nisisako, T.; Torii, T.; Higuchi, T. *Langmuir* **2004**, *20*, 9905−9908.

(24) According to the standards of the National Institute of Standards and Technology (NIST), a particle distribution may be considered monodispersed if at least 90% of the distribution lies within 5% of the median size (Particle Size Characterization. Special Publication 960-961, January 2001.

(25) Xia, Y.; Whitesides, G. M. *Angew. Chem., Int. Ed.* **1998**, *37*, 550−575.

(26) Huh, D.; Tung, Y. C.; Wei, H. H.; Grotberg, J. B.; Skerlos, S. J.; Kurabayashi, K.; Takayama, S. *Biomed. Microdevices* **2002**, *4*, 141−149.

Photopolymerization of the monomer droplets was carried out in a wavy channel of the microfluidic reactor (Figure 1b). Irradiation was carried out by using a UV-lamp (UVAPRINT 40C/CE, Dr. K. Hönle GmbH UV-Technologie, Germany), at a wavelength of 360 nm and an intensity at the sample location of 200 mW/cm^2. The distance between the lamp and the microfluidic chip was 15−20 cm. Figure 1c shows the core−shell droplets flowing in the serpentine channel. In the course of experiments regardless of the rate of production of droplets they were always separated with a gap of the continuous phase; thus, the droplets did not collide, and their coalescence was suppressed. Figure 1d shows a photograph of the microfluidic reactor for continuous synthesis of polymer capsules and particles with various shapes.

The generation of droplets from a liquid cylindrical jet occurred due to Rayleigh−Plateau hydrodynamic instability: under the action of interfacial tension the jet became unstable to perturbations with wavelengths larger than its circumference and reduced its surface area by breaking up into segments that acquired a spherical shape.[27] The dimensionless parameters describing the formation of droplets from the horizontally flowing jet are the Reynolds number $\boldsymbol{Re} \equiv \rho RU/\mu$ and the Capillary number $\boldsymbol{Ca} \equiv \mu U/\gamma_{12}$, where ρ, μ and U are the density, viscosity, and the average velocity of the liquid, respectively, γ_{12} is the interfacial tension, and R is a characteristic length scale of the system. We determined the Reynolds number as $\boldsymbol{Re} = \rho Q/\mu h$ where Q is the volume flow rate of the liquid and h is the height of the channel.[1,28] In our experiments the values of $\boldsymbol{Ca}$ and $\boldsymbol{Re}$ were in the range of $0.07 \leq Re_{drop} \leq 0.7$, $5 \times 10^{-3} \leq Ca_{drop} \leq 5 \times 10^{-2}$ (monomer phase) and $11 \leq Re_{cont} \leq 82$, $0.06 \leq Ca_{cont} \leq 0.5$ (continuous aqueous phase). The average diameter of the coaxial jet, d, in the equilibrium region was calculated using the continuity equation as [29] $d = [(4/\pi)(Q_{drop}/v_{x,cont})]^{1/2}$ (eq 1) where $v_{x,cont}$ is the velocity of the continuous phase in the center of the channel, $v_{x,cont} = 1.5Q_{cont}/A_{channel}$; Q_{drop}, and Q_{cont} are the flow rates of the droplet and continuous phases, respectively, and $A_{channel}$ is the area of cross-section of the downstream channel. The diameter, d_o, of droplets generated by break-up of the jet was determined by the value of interfacial capillary wavelength, $\lambda_{breakup}$, as $d_0 = (1.5\lambda_{breakup} d^2)^{1/3}$ (eq 2) where interfacial capillary wavelength is the length of the last wave within the coaxial jet before it broke up into droplets.[29,30]

Figure 2 shows the variation in jet diameter and the diameter of core−shell droplets with increasing flow rate of the continuous aqueous phase (the flow rates of monomer and oil phases were constant). In the course of experiments, the average diameter of the coaxial jet varied from 10 to 80 μm, in agreement with values of d calculated from eq 1 (Figure 2a). The average diameter of the core−shell droplets varied from 20 to 150 μm (Figure 2b), close to the values of d_o obtained from eq 2.

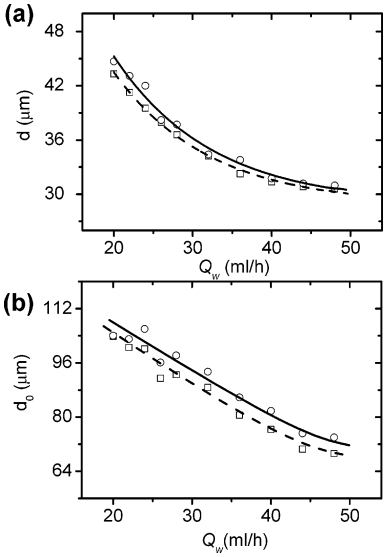

Figure 2. (a) Experimental (○) and calculated from eqs 1 and 2 (□) variation in average diameter of the coaxial jet and (b) average diameter of core−shell droplets plotted as a function of flow rate of the continuous phase Q_w for $Q_m = 0.30$ mL/h, $Q_o = 0.045$ mL/h. Solid and dashed lines are there to guide the eye.

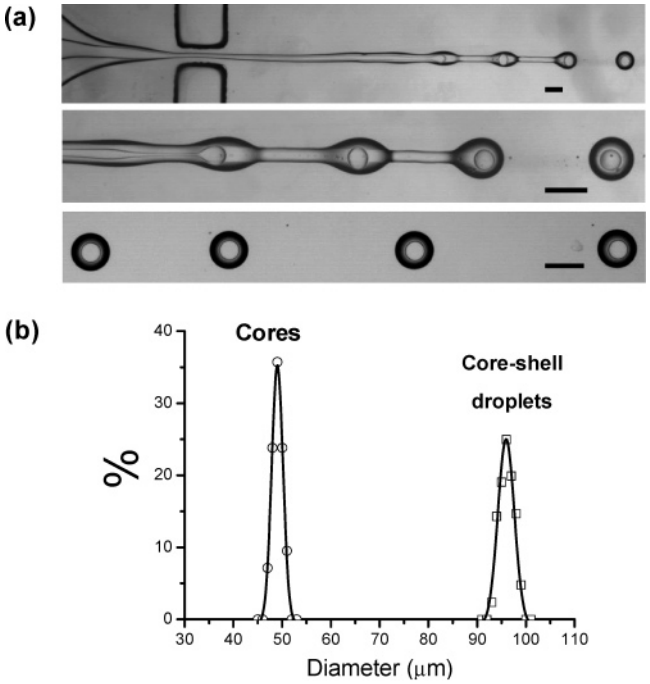

Figure 3. (a) Typical optical microscopy images of the break-up of a liquid jet formed by coaxial thread of silicone oil ($\eta = 10$ cst) and EGDMA, and the resulting core−shell droplets flowing in the downstream channel. (b) Size distributions of the SO cores and SO−EGDMA core−shell droplets obtained at $Q_w = 26$ mL/h, $Q_m = 0.30$ mL/h, and $Q_m = 0.045$ mL/h. Scale bar is 100 μm.

Figure 3a shows typical optical microscopy images of the periodically undulated coaxial oil−monomer jet and the resultant core−shell droplets. The core−shell droplets had a very narrow size distribution (Figure 3b). The coefficient of variance (defined as a standard deviation divided by the diameter of the droplets) was below 1.5% and 2.5% for the cores and the core−shell droplets, respectively. In the flow regimes reported in the present work we did not observe the formation of small satellite droplets.

(27) (a) Rayleigh, J. W. S. *Proc. London Math. Soc.* **1878**, *10*, 4-11. (b) Probstein, R. F. *Physicochemical Hydrodynamics*; Butterworth Publishers: Stoneham, MA, 1989. (c) Lin, S. P.; Reitz, R. D. *Annu. Rev. Fluid Mech.* **1998**, *30*, 85−105.
(28) Sugiura, S.; Nakajima, M.; Kumazawa, N.; Iwamoto, S.; Seki, M. *J. Phys. Chem. B* **2002**, *106*, 9405−9409.
(29) Cramer, C.; Berüter, B.; Fischer, P.; Windhab, E. J. *Chem. Eng. Technol.* **2002**, *25*, 499−506.
(30) Capillary wavelength is the distance between the corresponding points of two consecutive capillary waves originating from Rayleigh instability,[27] that is two points that have completed identical fractions of their periodic motion.

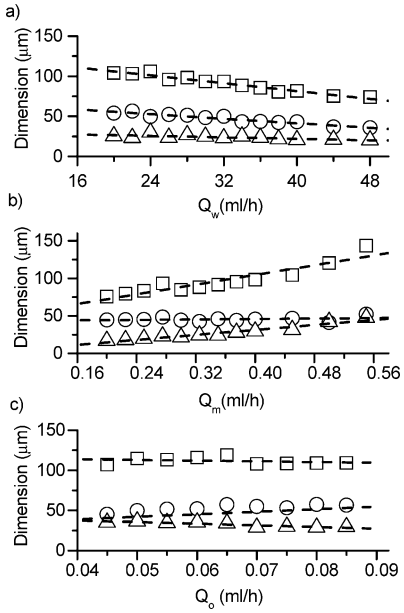

Figure 4. Variation in diameters of cores (○), core−shell droplets (□), and shell thicknesses (△) as a function of water flow rate, Q_w (a), EGDMA flow rate, Q_m (b) and SO (η = 10 cst) flow rate, Q_o (c). (a): Q_m = 0.30 mL/h, Q_o = 0.045 mL/h; (b): Q_w = 28 mL/h, Q_o = 0.045 mL/hr; (c) Q_m = 0.45 mL/h, Q_w = 28 mL/h. Dashed lines are there to guide the eye.

We varied the rates of flow of the oil, monomer, and aqueous phases (Q_o, Q_m, and Q_w, respectively) to control the diameter of cores, D_c, the size of core−shell droplets, D_o, and the thickness of shells, L, [$L = (D_o - D_c)/2$]. Figure 4a−c shows the effect of the variation in flow rates of the water, monomer, and oil phases on the values of D_c, D_o, and L. Generally, increase in ratio of flow rates of outer to inner phases (that is, water/monomer or monomer/oil) led to the reduction in size of droplets produced by the inner phase, due to the increasing shear stress imposed on the undulated jet of the dispersant liquid. Increase in the flow rate of the aqueous phase resulted in the formation of smaller droplets with smaller cores and thinner shells (Figure 4a). In Figure 4b with increasing monomer flow rate, the diameter of core−shell droplets increased, and the diameter of oil cores became smaller (thus resulting in thicker shells). At higher flow rates of the oil phase the diameter of cores increased, and the shell thickness decreased (Figure 4c). The overall size of core−shell droplets was only slightly affected, since the shear stress at the water/monomer interface remained almost invariant. Thus, by changing the flow rate of a particular liquid and keeping the flow rates of the other two liquids constant, we achieved precise control over the size of droplets, the diameter of cores, and the thickness of shells. Moreover, by changing flow rates of two nonadjacent liquids (water and oil) we achieved independent control over the size of cores and core−shell particles.

By changing the flow rates of three liquids we varied the values of interfacial capillary wavelengths and shifted the lengths and the phases of the capillary waves (undulations) with respect to each other. In this manner, we produced core−shell droplets with a different number, ***n***, of cores. Figure 5a shows a schematic of the approach to droplets with multiple cores. When the values of interfacial capillary wavelengths, $\lambda_{breakup,m}$ and $\lambda_{breakup,o}$[29] of the monomer and oil threads, respectively, were close and "in-phase", break-up of the coaxial jet produced droplets with a single oil core localized in the center of the droplet, Figure 5a, top. The core was aligned asymmetrically with respect to the droplet center when the capillary wavelengths

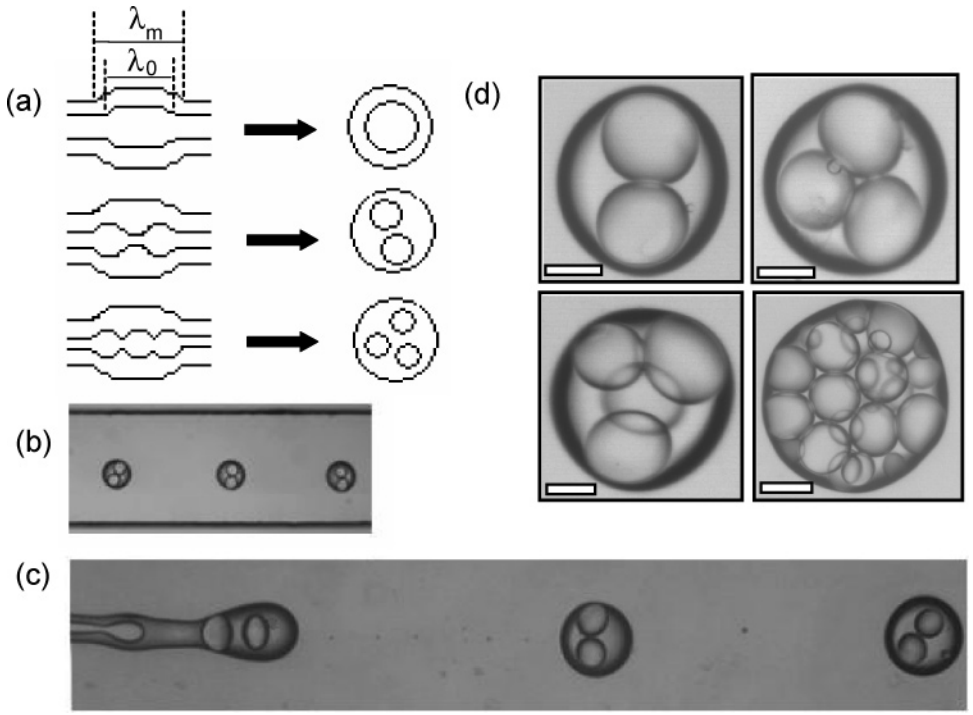

Figure 5. (a) Schematics of the formation of droplets with multiple cores. Inner phase: silicone oil, outer phase: monomer liquid. (b) Optical microscopy image of core−shell droplets with two cores flowing through the microfluidic device. (c) Break-up of the coaxial jet into two-core droplets. (d) Isolated core−shell droplets comprising a different number of SO cores engulfed with TPGDA shell. Conditions for the formation of core−shell droplets with two cores: Q_w = 8 mL/h, Q_m = 0.11 mL/h, Q_o = 0.052 mL/h; core−shell droplets with three cores: Q_w = 12 mL/h, Q_m = 0.16 mL/h, Q_o = 0.05 mL/h; core−shell droplet with four cores: Q_w = 9 mL/h, Q_m = 0.155 mL/h, Q_o = 0.054 mL/h; core−shell droplet with multiple cores: Q_w = 10 mL/h, Q_m = 0.165 mL/h, Q_o = 0.052 mL/h. Scale bar is 40 μm.

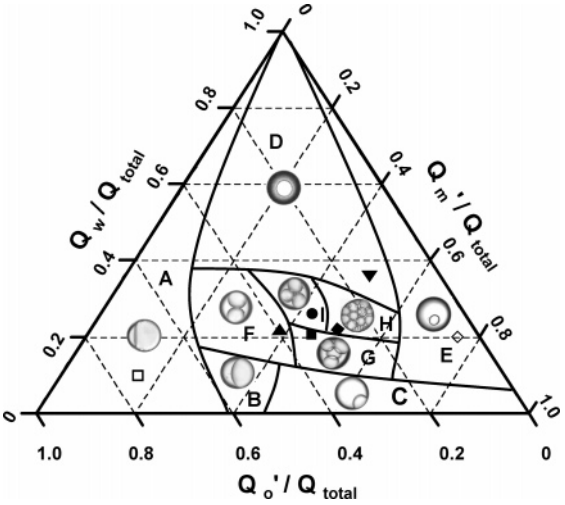

Figure 6. (a) Ternary phase-like diagram of hydrodynamic conditions used in the production of droplets with various morphologies. To accommodate all flow rate ratios on the same diagram we used $Q'_o = 240Q_o$, $Q'_m = 120Q_m$, $Q_{total} = Q'_o + Q'_m + Q_w$. Filled symbols correspond to hydrodynamic conditions used for the production of droplets shown in Figures 3a and 5d. Droplets with asymmetrically aligned core (△) were obtained at $Q_w = 18$ mL/h, $Q_m = 0.50$ mL/h, $Q_o = 0.012$ mL/h. Droplets with a small monomer inclusion adjacent to the oil surface (□) were produced at $Q_w = 6.0$ mL/h, $Q_m = 0.025$ mL/h, $Q_o = 0.20$ mL/h.

were "shifted in phase"; this configuration did not relax during photopolymerization.

Core−shell droplets with multiple cores formed for $\lambda_{breakup,m} > \lambda_{breakup,o}$, that is, when the frequency of the break-up of the oil thread exceeded the frequency of the break-up of the monomer thread, Figure 5a, middle and bottom. The cores were monodispersed when the value of $\lambda_{breakup,m}$ was commensurate to the integer number of $\lambda_{breakup,o}$. For $Q_m/Q_w \leq 0.02$ and $Q_o/Q_w \geq 0.003$ the number of oil cores increased with increasing flow rate of the monomer and/or decreasing flow rate of the oil. Figure 5b−d shows the break-up of the coaxial jet into core−shell droplets with two cores per droplet and typical optical microscopy images of isolated monomer droplets with a different number of oil cores. The fluid cores did not coalesce when they were engulfed with a monomeric shell.

Figure 6 shows a ternary "phase" diagram of hydrodynamic conditions for the production of core−shell droplets with different morphologies. To meet the requirement of ternary diagrams (that is, the sum of three variables is constant and equal to 1) we plotted on each axis the ratio of flow rate of a particular liquid (water, oil, or monomer phase) to the *total* flow rate of three liquids. We covered the whole range of flow rate ratios on the same diagram by using $Q'_o = 240Q_o$, $Q'_m = 120Q_m$, $Q_{total} = Q'_o + Q'_m + Q_w$. Filled symbols correspond to hydrodynamic conditions used for the generation of droplets in Figures 3a and 5d. In an early stage of evolution of a monomer droplet (and after close-to-complete emergence of an oil droplet), break-up of the jet produced droplets with a small monomer inclusion adjacent to the surface of oil droplet (region A). In the later stages of monomer droplet formation, the size of the monomer inclusion gradually increased (region B). Ultimately single-core droplets with classical core−shell morphologies evolved in a broad range of liquid flow rate ratios (region D). In an early stage of the evolution of an oil droplet, break-up of the jet produced droplets with a small oil inclusion adjacent to the surface monomer droplet (region C). Droplet morphology was also controlled by reducing the flow rate ratio Q'_o/Q_{total}: under these conditions an oil core in the core−shell droplets was misaligned with respect to the droplet center (region E). Droplets with multiple cores were obtained in regimes F−I.

We obtained polymer particles with different shapes by in situ photopolymerizing a monomer in the core−shell droplets and removing the silicone oil with acetone. The polymerization time was typically from 2 to 800 s. Conversion of monomer to polymer was close to 100%. Following polymerization the dimensions of the particles decreased by ca. 5−7%, in comparison with the corresponding droplets. No clogging of polymer particles occurred in the wavy channel. The productivity of the microfluidic reactor was from 200 to 1000 s^{-1}. Particle

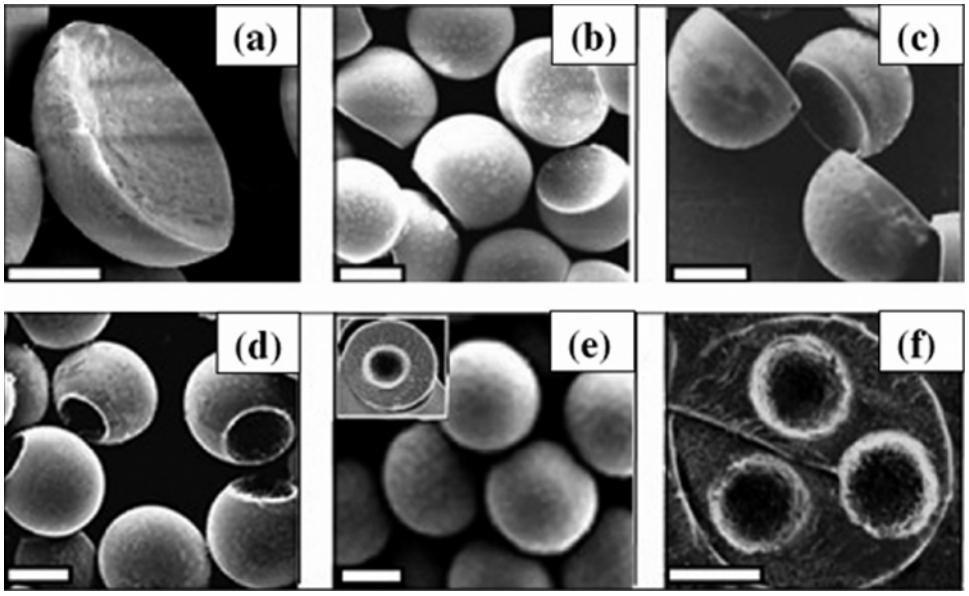

Figure 7. (a−e) Scanning electron microscopy images of polymer microbeads obtained by polymerizing TPGDA in droplets obtained in regimes A, B, C, D, respectively, after removing a SO core. (Inset) Cross section of the core−shell particle. (f) Cross section of a polyTPGDA particle with three cores obtained by polymerizing core−shell droplets with three cores (regime I in Figure 6). The particle is embedded in epoxy glue. Scale bar is 40 μm.

polydispersity did not exceed 2.5%, close to the polydispersity of the corresponding droplets.

Figure 7a−f shows typical SEM images of polyTPGDA particles. Truncated microspheres, hemispheres, particles with a "hole", and spherical capsules (Figure 7a−e) were obtained from the droplets obtained in regions A, B, C, and D, respectively, of the ternary diagram in Figure 6. Microspheres with three cores (Figure 7f) were obtained by polymerizing droplets obtained in region I. We stress that particles with various shapes and morphologies were obtained without changing the macroscopic properties of liquids (e.g., their viscosities and interfacial tensions). By contrast, with a thermodynamically driven control of droplet morphologies[17] careful variation of the hydrodynamic conditions and fast polymerization of the monomer phase allowed us to trap nonequilibrium shapes of droplets produced in the MFFD.

Conclusion

In conclusion, this work shows a new avenue for fast, scalable, continuous synthesis of polymer spherical capsules and particles with various shapes in continuous microfluidic reactors. The described strategy allows precise control of the emulsification process, leading to the production of monodispersed droplets (and the resulting particles) with controlled morphologies in the challenging size range from 20 to 200 μm. A small size and planar nature of the microfluidic devices allow for integration of many continuous microfluidics reactors on a single chip, thus increasing the quantity of particles produced per unit time. The microfluidic reactors can also be integrated with other microfluidic components such as valves and detectors placed on the same chip.[31]

Both monomers studied in the present work were efficiently used in the production of polymer particles with different shapes and morphologies. The proposed approach is not limited by the selection of nonpolar fluids for the generation of core−shell droplets. Core−shell droplets with aqueous or gaseous cores can be produced, if the values of interfacial tension and the ratios of fluid viscosities allow for the formation of core−shell droplets. Moreover, the combination of immiscible monomers in the core−shell droplets provides a route to the formation of Janus particles.[32]

Acknowledgment. The authors thank Prof. David James for useful discussions. E.K. thanks NSERC Canada for financial support of this work through the Canada Research Chair Fund.

Supporting Information Available: Experimental details. This material is available free of charge via the Internet at http://pubs.acs.org.

JA042494W

(31) Quake, S. R.; Scherer, A. *Science* **2000**, *290*, 1536−1539
(32) Paunov, V. N.; Carre, O. J. *Adv. Mater.* **2004**, *16*, 788−791.